(*The 39th International Workshop on Water Waves and Floating Bodies, 14-17 April 2024, St Andrews, Scotland*)

# Nonlinear free-surface responses in three-dimensional moonpools with recess

Xinshu Zhang*, Bei Chu

State Key Laboratory of Ocean Engineering, Shanghai Jiao Tong University, Shanghai 200240, China

## 1 Introduction

Moonpools refer to the vertical openings in drillships or offshore construction vessels (OCV). Moonpools are prone to resonance problems, under incident wave exciting and wave-induced motion of the floating structures. It's important to predict the natural frequencies, where the natural modes consist of piston mode and sloshing modes, the latter similar to that in the sloshing tank of a LNG ship. A few studies have been performed to predict the natural frequencies for moonpools without recess (Molin, 2001; Molin *et al.*, 2018; Tan *et al.*, 2019).

Some new moonpool design in drillships have "recesses", some kind of sub-compartments used, for assembling subsea equipments. Molin (2017) proposed a theoretical model to compute the natural frequencies for drillship with recess based on eigenfunction expansion method. In this model, the flow inside the moonpool is assumed to be two-dimensional such that piston mode and longitudinal sloshing mode can be considered.

On the other hand, the nonlinear responses inside moonpool or gap can be also critical as the amplitude of the nonlinear response can be much larger than the linear responses. Ravinthrakumar *et al.* (2020) investigated the moonpool responses on the vessel motion and the secondary resonances for three different moonpools. Zhao *et al.* (2017) studied the nonlinear gap resonance based on experiments in a wave basin and identify the different harmonics through phase separation method. Chu *et al.* (2022) investigated nonlinear response inside two-dimensional moonpool with recess using fully nonlinear potential flow method. By using the two-dimensional numerical wave tank based on CFD package STAR-CCM+ or OpenFOAM®, the higher harmonic components of the free-surface elevation in the narrow gap can be investigated with the damping effects considered automatically (see, e.g., Gao *et al.* (2019); Ding *et al.* (2022*a*,*b*)).

The above-mentioned studies on the nonlinear moonpool response focused on the cases without recess. The nonlinear behavior for three-dimensional moonpool with recess is still not clear. In the present study, we address the piston and sloshing modes in a relevant range of wave periods for a drillship in operational conditions in the South China Sea, and discuss how these influence the moonpool responses. A ship model with four different moonpool and recess sizes is investigated by performing model tests in the Ocean Basin at Shanghai Jiao Tong University. Major findings in the present study include the importance of secondary resonance and nonlinear behavior.

## 2 Semi-analytical model based on domain decomposition scheme

A domain-decomposition (DD) method is developed to determine the natural frequencies of the resonant modes in a three-dimensional moonpool with recess in deepwater. This is an extension of the method developed in Molin (2017) for moonpools with a three-dimensional flow field outside the moonpool and two-dimensional flow in the moonpool, whereas the present model in this study considers three-dimensional flow in the moonpool.

The sketch of the problem is shown in figure 2. The water depth is assumed to be infinite, and the beam and length of the drillship are taken to the limit when they are also infinite. This assumption works well for the

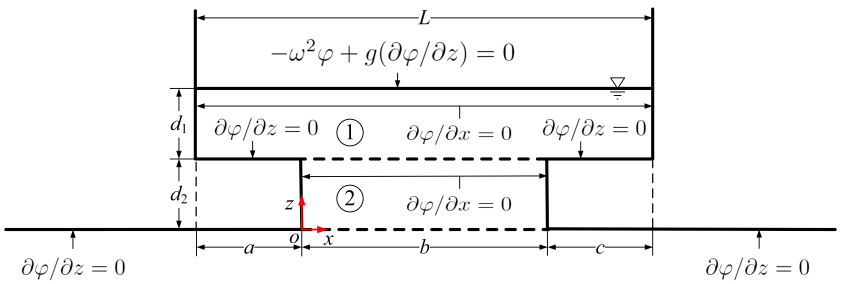


Figure 1: Boundary value problem for the domain-decomposition method with two subdomains, for determination of natural frequencies $\omega_{\mathrm{NM}}, \mathrm{N/M} = 0, 1, ..., \infty$.

*Presenting author

condition of infinite water depth. Three subdomains are defined and denoted in the sketch (figure 1), where the origin of the coordinate system is placed at the bottom left corner of the moonpool. It is assumed that velocity potential $\varphi$ satisfy the Laplace equation. The free-surface boundary condition is $g\varphi_z - \omega^2\varphi = 0$ at $z = d_1 + d_2$. The matching condition at $z = 0$ is written as

$$\varphi(x, y, 0) = \frac{1}{2\pi} \int_0^b \mathrm{d}x' \int_0^B \mathrm{d}y' \frac{\varphi_z(x, y, 0)}{\sqrt{(x - x')^2 + (y - y')^2}}. \tag{1}$$

The velocity potential in the subdomain 1 is taken as

$$\begin{aligned} \varphi_1(x, y, z) &= A_{00} + B_{00}\frac{z - d_2}{d_1} + \sum_{m=0}^{\infty} \sum_{\substack{n=0 \\ (m,n)\neq(0,0)}}^{\infty} [A_{mn} \cosh \nu_{mn}(z - d_2) \\ &\quad + B_{mn} \sinh \nu_{mn}(z - d_2)] \cos \lambda_m(x + a) \cos \mu_n y, \end{aligned} \tag{2}$$

with $\lambda_m = m\pi/L$, $\mu_n = n\pi/B$, $\nu_{mn}^2 = \lambda_m^2 + \mu_n^2$, where $m$ and $n$ are integers. The matrix $\mathbf{A}$ and $\mathbf{B}$ are the unknown coefficients.

In subdomain 2 that is located inside the recess, the velocity potential is written as

$$\begin{aligned} \varphi_2(x, y, z) &= C_{00} + D_{00}\frac{z}{d_2} + \sum_{p=0}^{\infty} \sum_{\substack{q=0 \\ (p,q)\neq(0,0)}}^{\infty} [C_{pq} \cosh \gamma_{pq} z \\ &\quad + D_{pq} \sinh \gamma_{pq} z] \cos \alpha_p x \cos \beta_q y, \end{aligned} \tag{3}$$

with $\alpha_p = p\pi/b$, $\beta_q = q\pi/B$. $p$ and $q$ are integers, and $\gamma_{pq}^2 = \alpha_p^2 + \beta_q^2$. The matrix $\mathbf{C}$ and $\mathbf{D}$ are the unknown coefficients.

The velocity potential and their derivatives should be matched on the common boundaries between subdomains 1 and 2 at $z = d_2$. In addition, $\varphi_2(x, y, z)$ should satisfy the boundary condition at $z = 0$. By substituting Eqn. (3) into Eqn. (1), we obtain the relation between $\mathbf{C}$ and $\mathbf{D}$. Finally the free-surface equation gives the relation for $\mathbf{A}$ and $\mathbf{B}$. Thus, by solving the final eigenvalue problem, we can obtain the natural frequencies and modal shapes for both longitudinal and transverse sloshing modes.

# 3 Experimental set-up

The experiments were carried out in the Deepwater Wave Basin at the Shanghai Jiao Tong University. This wave basin is 50 m long, 40 m wide, and the water depth can be adjusted from 0 to 10 m using an artificial bottom; here, the depth was set to 5 m. Flap-hinged wavemakers are fixed along two neighbouring sides of the basin and wave absorbing beaches are installed on the opposite sides to minimize the wave reflection from the boundaries of the basin.

As shown in figure 2, a ship with recessed moonpool (RMP) were used in the experiments. Four representative configurations are included. For the purpose of comparison, one moonpool without recess (also called RMP0) and three recessed moonpool configurations are considered and tested in the wave basin. RMP2, RMP3, RMP4 represent the recess lengths of 20 cm, 30 cm and 40 cm, respectively.

The ship was rigidly mounted on a gantry in the central area of the wave basin. The gantry is very robust, so provided enough stiffness to prevent vibration of the ship model at wave frequencies. The moonpool center was 25 m away from the wave paddles and 20 m from the sidewalls of the wave basin. A snapshot of the ship model is shown in figure 3, where both the gantry and the ship model are visible.

The experimental models represent 1 : 40 scaled versions of generalized but realistic vessels. Both white noise irregular wave and regular wave tests were carried out in the experiments. Ten wave gauges (WG 1 to WG 10) were placed inside the moonpool to measure the free-surface elevations with five WGs at each side.

# 4 Results and discussion

The natural modes and modal shapes obtained by solving the eigenvalue problem are compared with those from the experimental measurements under white noise irregular waves. The natural frequencies are summarized in Table 1. As shown in the table, the theoretical prediction for the natural frequencies of the first several resonant modes agree well those from the white noise test, particularly for the two sloshing modes.

Through the experiments around the piston mode frequencies, we obtained the free-surface response RAOs and different harmonics using FFT. Fig. 4 shows the typical time series of the wave elevation and amplitude spectra. As can be observed, as the recess length increases, the higher harmonics increase significantly. This can be explained by the fact that the first sloshing mode frequency decrease a little as the recess length $l$ increases from 20 cm to 40 cm (see Table 1). Another factor is that as the recess length increases, the piston mode resonance amplitude increases as well, as also observed in two-dimensional moonpool case with recess (Chu *et al.* (2022)), which induces more double-frequency components. More extensive results and analyses will be presented at the workshop.

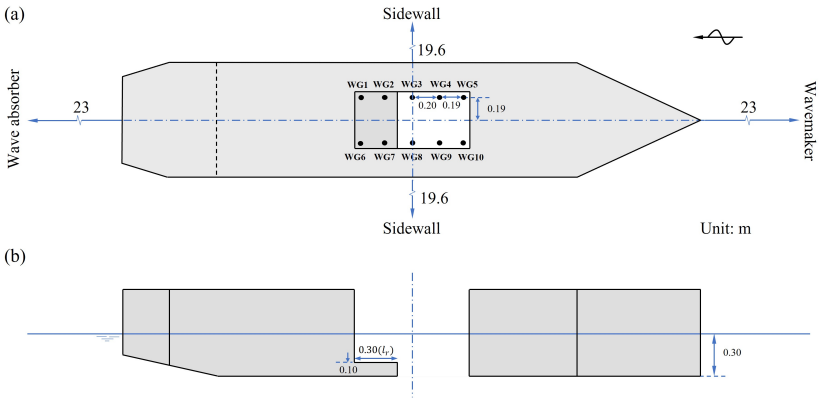


Figure 2: Sketch of a drillship with recessed moonpool in the wave basin under heading wave.

Figure 3: A snapshot of the drillship model (yellow) rigidly connected to the gantry (blue).

| Mode | 1 | 2 | 3 | 4 | 5 | 6 | 7 | 8 | 9 | 10 |
|---|---|---|---|---|---|---|---|---|---|---|
| RMP0 | | | | | | | | | | |
| Cal. (rad $s^{-1}$) | 4.2126 | 6.4121 | 8.7905 | 8.7915 | 9.2910 | 10.4391 | 10.7495 | 11.7837 | 12.4112 | 12.4112 |
| Meas. (rad $s^{-1}$) | 4.42 | 6.36 | 8.82 | | | | | | | |
| Dominant $(m, n)$ | (0, 0) | (1, 0) | (2, 0) | (0, 1) | (1, 1) | (2, 1) | (3, 0) | (3, 1) | (0, 2)+(2, 0) | (0, 2)-(2, 0) |
| RMP2 | | | | | | | | | | |
| Cal. (rad $s^{-1}$) | 3.7280 | 6.0244 | 8.6895 | 8.6904 | 9.2029 | 10.4088 | 10.7271 | 11.7749 | 12.4056 | 12.4060 |
| Meas. (rad $s^{-1}$) | 3.72 | 6.05 | 8.66 | | | | | | | |
| Dominant $(m, n)$ | (0, 0) | (1, 0) | (0, 1) | (2, 0) | (1, 1) | (2, 1) | (3, 0) | (3, 1) | (0, 2) | (4, 0) |
| RMP3 | | | | | | | | | | |
| Cal. (rad $s^{-1}$) | 3.3537 | 5.9015 | 8.6284 | 8.6730 | 9.1866 | 10.4028 | 10.7156 | 11.7688 | 12.4019 | 12.4025 |
| Meas. (rad $s^{-1}$) | 3.30 | 5.90 | 8.66 | | | | | | | |
| Dominant $(m, n)$ | (0, 0) | (1, 0) | (0, 1) | (2, 0) | (1, 1) | (2, 1) | (3, 0) | (3, 1) | (4, 0) | (0, 2) |
| RMP4 | | | | | | | | | | |
| Cal. (rad $s^{-1}$) | 2.9719 | 5.8516 | 8.5759 | 8.6277 | 9.1821 | 10.3834 | 10.6991 | 11.7628 | 12.3995 | 12.4002 |
| Meas. (rad $s^{-1}$) | 2.83 | 5.90 | 8.51 | | | | | | | |
| Dominant $(m, n)$ | (0, 0) | (1, 0) | (0, 1) | (2, 0) | (1, 1) | (2, 1) | (3, 0) | (3, 1) | (0, 2) | (4, 0) |

Table 1: Natural frequencies for one clean moonpool (RMP0) and three moonpools with a recess (RMP2, RMP3, RMP4).

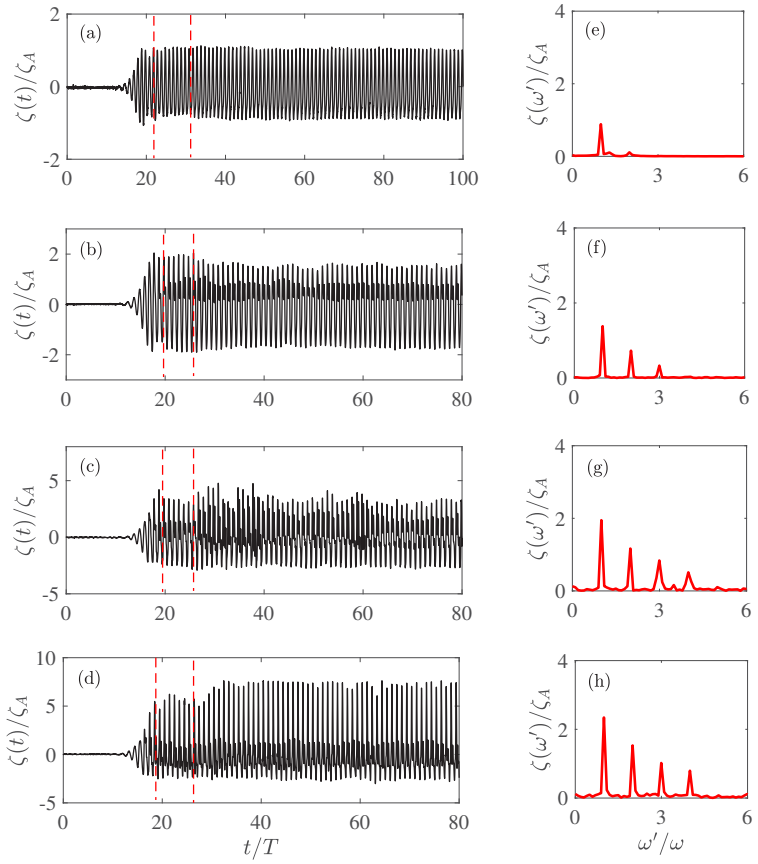


Figure 4: Time histories and spectra of WG1 at secondary resonances for the first longitudinal sloshing mode of the four different moonpools. ($a$, $e$) RMP0, $T = 1.95$ s; ($b$, $f$) RMP2, $T = 2.1$ s; ($c$, g) RMP3, $T = 2.1$ s; ($d$, $h$) RMP4, $T = 2.05$ s.

## Acknowledgement

The present work is sponsored by the National Natural Science Foundation of China under Grant No.52171269.

## References

Chu, B., Zhang, X. & Zhang, Y. 2022 Effects of nonlinearity and viscous damping on the resonant responses in two-dimensional moonpools with a recess. *Applied Ocean Research* **127**, 103295.

Ding, Y., Walther, J.H. & Shao, Y. 2022*a* Higher-order gap resonance and heave response of two side-by-side barges under stokes and cnoidal waves. *Ocean Engineering* **266**, 112835.

Ding, Y., Walther, J.H. & Shao, Y. 2022*b* Higher-order gap resonance between two identical fixed barges: A study on the effect of water depth. *Physics of Fluids* **34** (5), 052113.

Gao, J., Zang, J., Chen, L., Chen, Q., Ding, H. & Liu, Y. 2019 On hydrodynamic characteristics of gap resonance between two fixed bodies in close proximity. *Ocean Engineering* **173**, 28–44.

Molin, B. 2001 On the piston sloshing modes in moonpools. *J. Fluid Mech.* **430**, 27–50.

Molin, B. 2017 On natural modes in moonpools with recesses. *Appl. Ocean Res.* **67**, 1–8.

Molin, B., Zhang, X., Huang, H. & Remy, F. 2018 On natural modes in moonpools and gaps in finite depth. *J. Fluid Mech.* **840**, 530–554.

Ravinthrakumar, Senthuran, Kristiansen, Trygve, Molin, Bernard & Ommani, Babak 2020 Coupled vessel and moonpool responses in regular and irregular waves. *Applied Ocean Research* **96**, 102010.

Tan, L., Lu, L., Tang, G.-Q., Cheng, L. & Chen, X.-B. 2019 A viscous damping model for piston mode resonance. *J. Fluid Mech.* **871**, 510–533.

Zhao, W., Wolgamot, H., Taylor, P. & Taylor, R. 2017 Gap resonance and higher harmonics driven by focused transient wave groups. *J. Fluid Mech.* **812**, 905–939.